Anderson localization of cold atoms in a laser speckle disordered potential

Master 1 internship report
by Varvara Petrova

Laboratoire Matériaux et Phénomènes Quantiques
University Paris Diderot - Paris 7

August 29, 2016

Supervisor: Giuliano Orso
Reporter: Indranil Paul

Abstract

We study Anderson localization of cold atoms in one and two-dimensional optical speckle potentials. We compute a root-mean-square displacement using a split-step Fourier numerical method. We characterize its behaviour in non interacting regime and in the presence of synthetic Rashba-type spin-orbit coupling (for 2D systems). We also provide an estimate of localization length for 1D systems.

Contents

1 Introduction

It is known since the seminal work of Anderson (1958) that quantum interferences can completely suppress the diffusion of a particle in disordered medium, in spite of quantum tunnelling process and even if the particle is not localized classically [1]. This phenomenon is known as Anderson localization (AL). When the energy of the disorder strength is varied, the system can undergo a transition from the metallic phase with delocalized eigenstates to the insulating phase, where each eigenfunction $\psi_E(\boldsymbol{r})$ with energy E is exponentially localised:

$$|\psi_E(\boldsymbol{r})|^2 \propto \xi_E^{-d} e^{-|\boldsymbol{r}-\boldsymbol{r}_0|/\xi_E},\ |\boldsymbol{r}-\boldsymbol{r}_0| \gg \xi_E$$

where d is the dimensionality of the system, $\boldsymbol{r}_0$ is the localization center, ξ_E is the localization length at the energy E. The energy threshold separating localized from delocalized states is called mobility edge (E_c). Its location depends on the type and the strength of disorder.

A great progress in understanding of the corresponding physics was achieved in the seventies and eighties, due to the developments of the one-parameter scaling theory[1]. The theory predicts that [2], when the time-reversal and spin-rotation symmetries are preserved (in the absence of the magnetic field and spin-orbit coupling), in dimensions $d \leqslant 2$ all one-particle states are localized, and therefore no mobility edge exists, even if disorder is very weak. In dimensions $d > 2$ mobility edges do exist if the strength of disorder is weak enough, which implies the possibility for Anderson transitions.
According to the Ioffe–Regel criterion [3], Anderson transition occurs when the mean free path becomes comparable to the de Broglie wavelength or, equivalently, when the phase accumulated between two successive diffusions is of the order of 2π.
In the presence of spin-rotation coupling, the one-parameter scaling theory predicts the existence of Anderson transitions even in two dimension.

The scaling theory paved the way for the field-theoretical approaches to localization which demonstrated connections between the Anderson transition and conventional second order phase transitions. The physical observables whose scaling at the transition point is of primary importance [1] is the localization length ξ on the insulating side (say, $E < E_c$) and the DC-conductivity σ_{dc} on the metallic side ($E > E_c$):

$$\begin{aligned} \xi &\propto (E - E_c)^{-\nu} \\ \sigma_{dc} &\propto (E - E_c)^{s} \end{aligned}$$

where the critical indices ν and s satisfy $s = \nu(d-2)$. The divergence of ξ as $E \to E_c$ reveals the universal nature of AL i.e. independently of microscopic details, it develops in a similar way in apparently different systems, governed by different equations. AL is in essence a wave phenomenon. Among others, it has been reported for light waves

[1]The theory describes the flow of the dimensionless conductance $g(L)$ with the linear size of the system L: $\frac{\mathrm{d}\ln g}{\mathrm{d}\ln L} = \beta(g)$. $\beta(g)$ is independent of L but depends on the model one studies.

in diffusive media [4, 5] or photonic crystals [6, 7], sound waves [8], microwaves [9] and cold atomic gas (Bose-Einstein condensate) [10].

In the present paper, we consider a cold atomic gas in random optical potential. Such a system has many advantages, among them are [11, 12]:

- Small atom-atom interaction effects in low density regime. In the high-density regime, single-particle dynamics can be studied by reducing the scattering length via Feshbach resonances, eventually reaching the ideal Bose gas regime.
- Interference effects at the origin of AL can be preserved over a relatively long time.
- The spatial and temporal typical scales are convenient for a direct observation of the localization.
- It can be used to realize condensed matter model systems.

We study its dynamics in one (1D) and two dimensions (2D) and explore the possibility of Anderson transition in the presence of synthetic Rashba-type spin-orbit coupling.

2 Framework

To begin with, we consider a system of non interacting cold atoms of mass m, subjected to a random potential $V(\boldsymbol{r})$. Its dynamics is governed by the single-particle Hamiltonian:

$$\hat{H} = \frac{\hat{\boldsymbol{p}}^2}{2m} + V(\boldsymbol{r}) \tag{1}$$

where $\hat{\boldsymbol{p}} = -i\hbar\nabla$. The coordinate vector $\boldsymbol{r}$ belongs to a d-dimensional finite-size domain $\left[-\frac{L}{2}, \frac{L}{2}\right]^d$ with $d = 1, 2$.
In practice, optical speckle potentials are obtained by monochromatic illumination of a medium with a random phase profile, such as a ground glass plate [13], or a holographic phase mask [12]. The resulting potential $V(\boldsymbol{r})$ felt by atoms subjected to this light derives from the Gaussian random field $\mathcal{E}(\boldsymbol{r})$, but is not a Gaussian variable by itself (see §5.1). The sign of V depends on the laser detuning. Preshifted for convenience by its average value so that $\langle V \rangle = 0$, the potential has the following on-site distribution [14]:

$$P(V) = \frac{1}{V_0}\Theta(V_0 \pm V) \exp\left(-\frac{V_0 \pm V}{V_0}\right) \tag{2}$$

where Θ is the Heavside function and $V_0 > 0$ is the disorder strength related to the variance by $\langle V^2 \rangle = V_0^2$. In Eq. (2), the upper sign refers to a blue detuned speckle potential, bounded by $-V_0$ from below, and the lower sign to a red-detuned speckle potential bounded by V_0 from above.

Optical speckles (potential bumps) have a non zero spatial extension with a typical grain size of the order of 1 µm [15]. This aspect is modelled by a two-point correlation function $G(\boldsymbol{r}, \boldsymbol{r}') = \langle V(\boldsymbol{r})V(\boldsymbol{r}') \rangle$. The two-point correlation function can take

various forms depending on the experimental setup[2]. In the present work, we consider an isotropic speckles which correlation function depends only on $\|\boldsymbol{r}-\boldsymbol{r'}\|$ and decays over a typical distance σ in d dimensions as follows:

$$G(r) = \langle V(\boldsymbol{r}')V(\boldsymbol{r}'+\boldsymbol{r})\rangle = V_0^2\left[C_d\left(\frac{r}{\sigma}\right)\right]^2 \tag{3}$$

where the function C_d is defined by:

$$C_d(r) = \begin{cases} \frac{\sin(r)}{r} & \text{for} \quad d=1 \\ \frac{2J_1(r)}{r} & \text{for} \quad d=2 \end{cases}$$

J_1 being the first order Bessel function of the first kind.
σ is referred to as the correlation length. It defines the intrinsic physical scale of our system. In turn, it also defines a characteristic energy scale for the atomic dynamics, the so-called correlation energy:

$$E_\sigma = \frac{\hbar^2}{2m\sigma^2}$$

The rescaling $\boldsymbol{r} \to \frac{\boldsymbol{r}}{\sigma}$ (or $\boldsymbol{k} \to \boldsymbol{k}\sigma$), $t \to \frac{tE_\sigma}{\hbar}$ and $\psi \to \psi\sigma^{d/2}$ allows us to write the time-dependent Schrödinger equation $i\hbar\partial_t\psi = \hat{H}\psi$ in dimensionless form:

$$i\partial_t\psi(\boldsymbol{r},t) = \left[\boldsymbol{k}^2 + V(\boldsymbol{r})\right]\psi(\boldsymbol{r},t) \tag{4}$$

where V is measured in units of E_σ.

For two-dimensional system in (x,y)-plane in the presence of (synthetic) spin-orbit interaction of Rashba type, the full Hamiltonian writes [16]:

$$\hat{H} = \frac{\hat{\boldsymbol{p}}^2}{2m} + V(\boldsymbol{r}) + \frac{\lambda_R}{\hbar}\left(\hat{p}_y\hat{\sigma}_x - \hat{p}_x\hat{\sigma}_y\right) \tag{5}$$

where $\lambda_R > 0$ is the strength of Rashba coupling and $\hat{\sigma}_x, \hat{\sigma}_y$ are the Pauli spin matrices. Applying the same rescaling as described above, we find the dimensionless form of the corresponding Schrödinger equation:

$$i\partial_t\psi(\boldsymbol{r},t) = \left[\boldsymbol{k}^2 + V(\boldsymbol{r}) + \lambda\left(\hat{k}_y\hat{\sigma}_x - \hat{k}_x\hat{\sigma}_y\right)\right]\psi(\boldsymbol{r},t) \tag{6}$$

where ψ is now a two component spinor denoted by:

$$\psi = \begin{pmatrix}\psi_+ \\ \psi_-\end{pmatrix}$$

[2]It may be shown that models with finite-range and/or anisotropic disorder correlations are equivalent with respect to white noise model with renormalized parameters [1]. The white nose model corresponds to $G(\boldsymbol{r},\boldsymbol{r}') = (2\pi\rho\tau)^{-1}\,\delta\left(\boldsymbol{r}-\boldsymbol{r}'\right)$, where ρ and τ are respectively the density of states and free time.

and $\lambda = \frac{\lambda_R}{\sigma E_\sigma}$. Notice that without disorder potential ($V = 0$), the Hamiltonian $\hat{H}_{RS0} = \hat{\boldsymbol{k}}^2 + \lambda\left(\hat{k}_y\hat{\sigma}_x - \hat{k}_x\hat{\sigma}_y\right)$ is diagonalizable. One can find its two eigenvalues $\lambda_\pm(\boldsymbol{k}) = \boldsymbol{k}^2 \pm \lambda k$ with respective eigenvectors given by:

$$\chi_\pm(\boldsymbol{k}) = \frac{1}{\sqrt{2}}\begin{pmatrix} \pm i e^{-i\theta_{\boldsymbol{k}}} \\ 1 \end{pmatrix}$$

where $k = \|\boldsymbol{k}\| = \sqrt{\left(k_x^2 + k_y^2\right)}$ and $\theta_{\boldsymbol{k}} = \arctan\left(\frac{k_y}{k_x}\right)$. As we shall see in the next section, this result can be used to solve the Eq. (6) by time-splitting numerical methods.

3 Project objectives

In this project we study the dynamics of an atomic wave-packet in the presence of the disorder potential. We numerically compute the time-dependent average size $\ell(t) = \sqrt{\langle \boldsymbol{r}^2 \rangle}$ of the wave-packet ψ, where $\langle \boldsymbol{r}^2 \rangle = \langle \psi | \boldsymbol{r}^2 | \psi \rangle$ and verify that:

$$\lim_{t \to +\infty} \ell(t) - \ell(0) = \begin{cases} \text{Cst} & \text{for localized states} \\ \sqrt{Dt} & \text{for extended states, where D is the diffusion constant.} \end{cases}$$

We shall check that numerical solution ψ is norm- and energy-preserving so that $\langle \psi | \psi \rangle = \int \mathrm{d}^d \boldsymbol{r} |\psi(\boldsymbol{r}, t)|^2 = \langle \psi_0 | \psi_0 \rangle \ \forall t$ and ${}_t\langle \psi | \hat{H} | \psi \rangle_t = \langle \psi_0 | \hat{H} | \psi_0 \rangle \ \forall t$, where ψ_0 is the initial state.

4 Numerical methods

To solve the Eq. (4) and (6), we use the so called split-step fast Fourier transform method (SS-FFT), which belongs to the family of pseudo-spectral methods [17] used to solve time dependent nonlinear partial differential equations (PDE). The nonlinear PDE is devided into related sub-problems of the original equation. To illustrate the method, we consider the Eq. (4) in one dimension:

$$i\partial_t \psi(x,t) = \left[-\partial_{xx} + V(x)\right]\psi(x,t), \quad -\tfrac{L}{2} \leqslant x < \tfrac{L}{2}, \quad 0 \leqslant t < t_{max}$$

and assume the following initial condition:

$$\psi(x,0) = \psi_0(x), \quad -\tfrac{L}{2} \leqslant x < \tfrac{L}{2}$$

We discretize the space domain of size L into M equal-sized intervals Δx so that $L = M\Delta x$. L must be sufficiently large to ensure that $\mathrm{supp}(\psi) \subsetneq \left[-\frac{L}{2}, \frac{L}{2}\right)$ in the time interval studied. We choose the step size $\Delta x = \eta\pi$ with $\eta = 0.2$ unless otherwise specified. As suggested in [11], the value $\eta = 0.2$ is small enough to resolve the details of the disordered potential and the oscillations of the wave function, that is in particular smaller than σ. In order to optimize the efficacy of the fft algorithm, we set M be equal to a power of

two. The corresponding step size in momentum space in given by $\Delta k = \frac{2\pi}{L}$. We also fix the time step size Δt and let the grid points and time steps be:

$$\begin{cases} x_n &= n\Delta x & n = -\frac{M}{2}, -\frac{M}{2}+1, ..., \frac{M}{2}-1 \\ k_m &= m\Delta k & m = -\frac{M}{2}, -\frac{M}{2}+1, ..., \frac{M}{2}-1 \\ t_q &= q\Delta t & q = 0, 1, ..., Q-1 \end{cases}$$

Let ψ_n^q be the numerical approximation of $\psi(x_n, t_q)$ and $\widehat{\psi}_m^q$ that one of the Fourier transform of ψ at point (k_m, t_q). We use the following definitions of the Fourier transform (FT) and its inverse (FT^{-1})

$$FT: \quad \widehat{f}(k) = \int_{-\infty}^{+\infty} f(x) e^{-ikx} \mathrm{d}x$$
$$FT^{-1}: \quad f(x) = \tfrac{1}{2\pi} \int_{-\infty}^{+\infty} \widehat{f}(k) e^{ikx} \mathrm{d}k$$

We decompose the Hamiltonian $H = -\partial_{xx} + V(x)$ into the kinetic energy part $T = -\partial_{xx}$ and the potential energy part V. Given a solution at time t, say $\psi(x,t)$, one can find the approximate solution at time $t + \Delta t$ by applying the infinitesimal time evolution operator $e^{-iH\Delta t}$, splitted up in the following symmetric[3] way [18]:

$$e^{-iH\Delta t} = e^{-i(V+T)\Delta t} \approx e^{-iV\frac{\Delta t}{2}} e^{-iT\Delta t} e^{-iV\frac{\Delta t}{2}}$$

One can show, using the Baker-Campbell-Housdorff formula, that the error associated to this development is proportional to $e^{\mathcal{O}(\Delta t^3)}$ and thus can be made negligible for sufficiently short time steps Δt. In the general case, an efficient calculation of the propagator $e^{-iH\Delta t}$ is possible if the operators T and V are diagonal in momentum space resp. real space. Consequently, $e^{-iV\frac{\Delta t}{2}}\psi$ will be calculated in real space whereas $e^{-iT\Delta t}\widehat{\psi}$ in momentum space, where $e^{-iT\Delta t}$ is identified with the simple multiplication by $e^{-ik^2\Delta t}$. Between these under-steps one has to Fourier transform and inverse transform the wavefunction, which can be done using the fast Fourier transform algorithm.

The following pseudocode resumes the steps to be followed:

$\psi^0(x) \leftarrow \psi_0(x)$
for $q \leftarrow 0$ **to** $Q-1$ **do**
  $\psi^{(a)}(x) \leftarrow \psi^q(x) e^{-iV(x)\frac{\Delta t}{2}}$
  $\widehat{\psi}^{(b)}(k) \leftarrow \widehat{\psi}^{(a)}(k) e^{-ik^2\Delta t}$
  $\psi^{q+1}(x) \leftarrow \psi^{(b)}(x) e^{-iV(x)\frac{\Delta t}{2}}$
end

[3]The propagator $e^{-i(V+T)\Delta t}$ can also be approximated by:

$$e^{-i(V+T)\Delta t} = e^{-iV\Delta t} e^{-iT\Delta t} e^{\frac{1}{2}[V,T]\Delta t^2 + \mathcal{O}(\Delta t^3)} \approx e^{-iV\Delta t} e^{-iT\Delta t}$$

making thus an error on the order of $e^{\mathcal{O}(\Delta t^2)}$.

where $\psi^{(a)}$ and $\psi^{(b)}$ designate the intermediate results, updated at each time step.

Notice that the unitarity of the propagator guarantees that the total probability of presence $\langle\psi|\psi\rangle$ is preserved.
Generalizations to dimension 2 (and higher, if necessary) are straightforward for tensor product grids and the results remain valid without modifications.

The same approach can be used to solve the Eq. (6) involving the spin-orbit coupling term. We start by decomposing the Hamiltonian into two parts:

$$W = \begin{pmatrix} V & 0 \\ 0 & V \end{pmatrix} \quad \text{and} \quad T = \begin{pmatrix} \boldsymbol{k}^2 & \lambda(k_y + ik_x) \\ \lambda(k_y - ik_x) & \boldsymbol{k}^2 \end{pmatrix}$$

From the previous section we have the spectrum of the matrix T, $\mathrm{Spec}(T) = \{\lambda_\pm\}$, with corresponding orthonormal eigenvectors $\chi_\pm$. Let $\widehat{\psi}(\boldsymbol{k}, t)$ be a two-component spinor wavefunction in momentum space. Its decomposition in the eigenbasis writes:

$$\widehat{\psi}(\boldsymbol{k}, t) = \begin{pmatrix} \widehat{\psi}_+(\boldsymbol{k}, t) \\ \widehat{\psi}_-(\boldsymbol{k}, t) \end{pmatrix} = \alpha(\boldsymbol{k}, t)\chi_+(\boldsymbol{k}, t) + \beta(\boldsymbol{k}, t)\chi_-(\boldsymbol{k})$$

where

$$\begin{aligned} \alpha(\boldsymbol{k}, t) &= \chi_+^\dagger(\boldsymbol{k})\widehat{\psi}(\boldsymbol{k}, t) = \tfrac{1}{\sqrt{2}}\left(-ie^{i\theta_{\boldsymbol{k}}}\widehat{\psi}_+(\boldsymbol{k}, t) + \widehat{\psi}_-(\boldsymbol{k}, t)\right) \\ \beta(\boldsymbol{k}, t) &= \chi_-^\dagger(\boldsymbol{k})\widehat{\psi}(\boldsymbol{k}, t) = \tfrac{1}{\sqrt{2}}\left(ie^{i\theta_{\boldsymbol{k}}}\widehat{\psi}_+(\boldsymbol{k}, t) + \widehat{\psi}_-(\boldsymbol{k}, t)\right) \end{aligned}$$

It follows that:

$$e^{-iT\Delta t}\widehat{\psi}(\boldsymbol{k}, t) = \alpha(\boldsymbol{k}, t)e^{-i\lambda_+\Delta t}\chi_+(\boldsymbol{k}, t) + \beta(\boldsymbol{k}, t)e^{-i\lambda_-\Delta t}\chi_-(\boldsymbol{k})$$

The split-step scheme thus becomes:

$\psi_+^0(x) \leftarrow \psi_0(x)$;
$\psi_-^0(x) \leftarrow \phi_0(x)$
for $q \leftarrow 0$ **to** $Q - 1$ **do**
  $\psi_+^{(a)}(\boldsymbol{r}) \leftarrow \psi_+^q(\boldsymbol{r})e^{-iV(\boldsymbol{r})\frac{\Delta t}{2}}$;
  $\psi_-^{(a)}(\boldsymbol{r}) \leftarrow \psi_-^q(\boldsymbol{r})e^{-iV(\boldsymbol{r})\frac{\Delta t}{2}}$;
  $\widehat{\psi}_+^{(b)}(\boldsymbol{k}) \leftarrow \frac{ie^{-i\theta_{\boldsymbol{k}}}}{\sqrt{2}}\left(\alpha^q(\boldsymbol{k})e^{-i\lambda_+\Delta t} - \beta^q(\boldsymbol{k})e^{-i\lambda_-\Delta t}\right)$;
  $\widehat{\psi}_-^{(b)}(\boldsymbol{k}) \leftarrow \frac{1}{\sqrt{2}}\left(\alpha^q(\boldsymbol{k})e^{-i\lambda_+\Delta t} + \beta^q(\boldsymbol{k})e^{-i\lambda_-\Delta t}\right)$;
  $\psi_+^{q+1}(\boldsymbol{r}) \leftarrow \psi_+^{(b)}(\boldsymbol{r})e^{-iV(\boldsymbol{r})\frac{\Delta t}{2}}$;
  $\psi_-^{q+1}(\boldsymbol{r}) \leftarrow \psi_-^{(b)}(\boldsymbol{r})e^{-iV(\boldsymbol{r})\frac{\Delta t}{2}}$;
end

Here we have set $\alpha^q(\boldsymbol{k}) = \chi_+^\dagger\widehat{\psi}^{(a)}(\boldsymbol{k})$ and $\beta^q(\boldsymbol{k}) = \chi_-^\dagger\widehat{\psi}^{(a)}(\boldsymbol{k})$ with $\widehat{\psi}^{(a)} = \begin{pmatrix} \widehat{\psi}_+^{(a)} \\ \widehat{\psi}_-^{(a)} \end{pmatrix}$

5 Numerical results and discussion

5.1 Speckle potential

To generate a speckle potential, both in one and two dimensions as depicted in Fig. 1, we use a numerical procedure that is rather close to the experimental scenario.

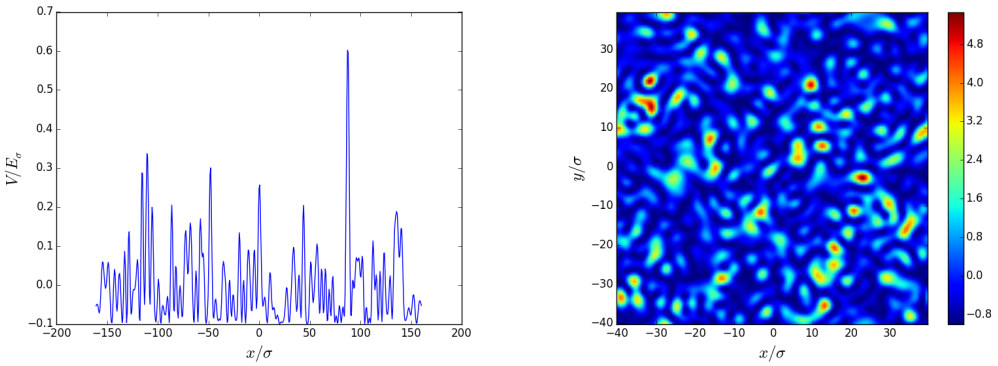

(a) d=1. $M = 512$ (b) d=2. $M = 128$.

Fig. 1: Numerical realizations of a blue-detuned 1D and 2D speckle potential.

We first generate a spatially uncorrelated (dimensionless) electric field $\mathcal{E}(\boldsymbol{r}) = a(\boldsymbol{r}) + ib(\boldsymbol{r})$ where $a(\boldsymbol{r})$ and $b(\boldsymbol{r})$ are independent random variables following the standard normal distribution. The field $\mathcal{E}$ is then multiplied in Fourier space by a proper cut-off function that physically describes the shape of the speckle pattern. The Heaviside cut-off function $\Theta(k_0 - \|\boldsymbol{k}\|)$ with $k_0 = 1$ (in units of σ^{-1}) allows to reproduce the two-point correlation function introduced in §2. It reflects the fact that the potential is smooth on length scales smaller than σ, but uncorrelated on distances larger than σ. We thus obtain a spatially correlated complex field

$$\mathcal{E}'(\boldsymbol{r}) = (2\pi)^{-d} \int_{\mathbb{R}^d} \mathrm{d}^d \boldsymbol{k}\, \widehat{\mathcal{E}}(\boldsymbol{k}) \Theta(k_0 - \|\boldsymbol{k}\|) e^{i\boldsymbol{k}\boldsymbol{r}}$$

Setting $V' = |\mathcal{E}'|^2$, shifting it by its average value and renormalizing the result, we finally obtain the desired potential V:

$$V(\boldsymbol{r}) = \left(\frac{V'(\boldsymbol{r})}{\langle V' \rangle} - 1 \right) V_0$$

Here, the average over all possible realizations of disorder $\langle ... \rangle$ was likened to the average over the space for the considered realisation of V' i.e. $\langle V' \rangle \approx \frac{1}{M^d} \sum_{\boldsymbol{j}} V'(\boldsymbol{r}_{\boldsymbol{j}})$. Using the same approach, we find that V has a mean of zero, within 10^{-15}, and a variance of V_0^2 with the absolute error of the order of 0.01 in two dimensions and 0.1 in one dimension.

A histogram plotted in Fig. 2 shows that the blue-detuned potential V constructed in this way follows the expected distribution low $P(V)$ given in the Eq. (2). Averaging over N=30 or more realizations of V and/or enlarging the system size are necessary, especially in one dimension, to improve and smooth the convergence.

The Fig. 3 illustrates the behaviour in the neighbourhood of zero of the correlation function $G_d(r) = \langle V(\boldsymbol{r}')V(\boldsymbol{r}'+\boldsymbol{r})\rangle$ calculated using the following approximations:

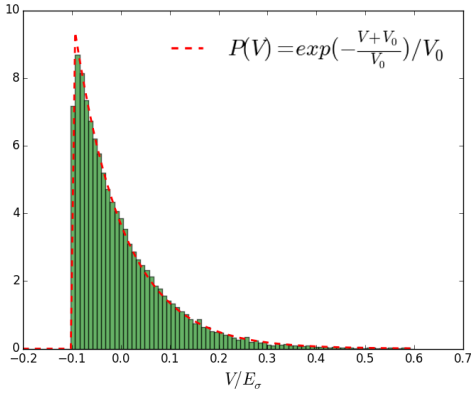

Fig. 2: Histogram of V, averaged over 50 disorder realizations in one dimension (M=512, V_0=0.1) and its comparison to the distribution law of a blue-detuned speckle potential. Similar result is obtained for *one* realization of V in two dimensions.

$$G_1(r) \approx \frac{1}{N_1(r)} \sum_{|x-x'|=r} V(x)V(x')$$

$$G_2(r) \approx \frac{1}{2N_2(r)} \left(\sum_x \sum_{|y-y'|=r} V(x,y)V(x,y') + \sum_y \sum_{|x-x'|=r} V(x,y)V(x',y) \right)$$

where $N_1(r) = \mathrm{Card}\{(x,x') \ / \ |x-x'| = r\}$ and $N_2(r) = MN_1(r)$. Averaged over a few dozen (few hundreds) realizations of disorder for 2D (resp. 1D) systems – the obtained functions are in agreement with expected analytical results (see Eq. (3)). The convergence is less accurate at large r, where the statistic is impoverished by the finite-size of the system and our rough approximation. The mean absolute convergence error for d=1 (M=512) at $r \gg 1$, which is of the order of 0.005 as well as after 200 as after 1000 realizations of disorder, may be reduced by enlarging the system size. Decreasing the step size $\Delta x = \eta\pi$ (taking $\eta = 0.1,\ 0.05$ or less instead of 0.2) keeping the system size unchanged, turns out to be ineffective for this purpose.

5.2 Localization in 1D and 2D without spin-orbit interaction

Initially prepared in a state described by a Gaussian wave packet:

$$\psi_0(x) = \sqrt{C} e^{-\frac{x^2}{2\sigma_g^2}} \quad \text{for d=1} \tag{7}$$

$$\psi_0(x,y) = C e^{-\frac{x^2+y^2}{2\sigma_g^2}} \quad \text{for d=2} \tag{8}$$

with $C = (\sqrt{\pi}\sigma_g)^{-1}$ so that $\langle\psi_0|\psi_0\rangle = 1$, the system is left to evolve in the presence of the disorder according to the Eq.(4). For a given choice of the disorder strength V_0 (quantum regime implies that $V_0 \leqslant 1$) and the width of the initial Gaussian wave packet, the root-mean-square displacement $\ell(t) = \sqrt{t\langle\psi|\boldsymbol{r}^2|\psi\rangle_t}$ is calculated. In the following, ℓ_{lim} denotes the limit of $\ell(t)$ as $t \to +\infty$, if it exists.

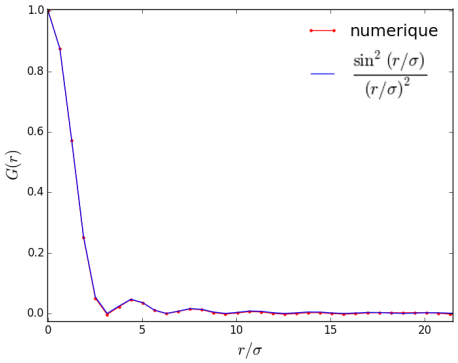

(a) d=1. $M = 4096$. N=200

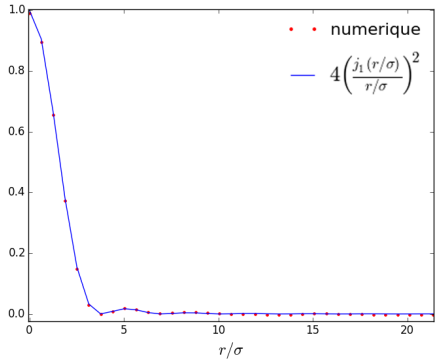

(b) d=2. $M = 256$. N=30

Fig. 3: Correlation functions in the neighbourhood of zero for d=1,2, $V_0 = 1$ for N realizations of disorder and their comparison with the analytical results.

In the absence of the disorder, one can observe a ballistic expansion of the initial wavepacket (both in 1D and 2D), with the root-mean-square deviation increasing linearly with time, as expected analytically[4].
As shown in figure 4(a), obtained for a given realization of disorder in one dimension, the presence of random potential impedes the wavepacket spread, containing it in a static exponential envelope of the form $\frac{1}{\xi}e^{-\frac{|x|}{\xi}}$. The localization length ξ was estimated to be equal to $0.7\ell_{lim}$ – this is a general observation for one-dimensional systems in the described configuration.

Figures 4(b) and 4(c) suggest the asymptotic behaviour of the function $\ell(t)$ as $t \to +\infty$. It is particularly obvious under the strong disorder ($V_0 \sim 1$) and in one dimensional systems. The convergence of $\ell(t)$ to a constant is difficult to prove numerically for week disorder, especially for 2D-systems, as it requires an infinitely long time integration interval and infinitely large system size to satisfy the condition $\lim_{|\boldsymbol{r}|\to\pm\frac{L}{2}} \psi(\boldsymbol{r}, t) = 0$, $\forall t$.

The existence of fluctuations in the function $\ell(t)$ – as those in figure 4(b) for $V_0 \geqslant 0.5$

[4] One can show, using the definition of the Fourier transform (see page 5 for the convention used) and the integral representation of the delta function $\left(\delta_d(\boldsymbol{r}-\boldsymbol{r}_0) = (2\pi)^{-d}\int_{\mathbb{R}^d} \mathrm{d}^d\boldsymbol{k} e^{i(r-r_0)k}\right)$, that:

$$\ell^2(t) = \int_{\mathbb{R}^d} \mathrm{d}\boldsymbol{r}\boldsymbol{r}^2|\psi(\boldsymbol{r},t)|^2 = (2\pi)^{-d}\int_{\mathbb{R}^d} \mathrm{d}\boldsymbol{k}|\nabla_{\boldsymbol{k}}\widehat{\psi}(\boldsymbol{k},t)|^2 \tag{9}$$

From the assumption that the Hamiltonian $H = \boldsymbol{k}^2$ ($V = 0$), we get $\widehat{\psi}(\boldsymbol{k},t) = e^{-i\boldsymbol{k}^2 t}\widehat{\psi}_0(\boldsymbol{k})$. By plugging this expression into (9) we obtain, after calculation:

$$\ell^2(t) = \alpha t^2 + 2it(2\pi)^{-d}\int_{\mathbb{R}^d} \mathrm{d}\boldsymbol{k}\boldsymbol{k}\boldsymbol{j} + \ell^2(0)$$

where $\alpha = 4(2\pi)^{-d}\int_{\mathbb{R}^d} \mathrm{d}\boldsymbol{k}\boldsymbol{k}^2|\widehat{\psi}_0(\boldsymbol{k})|^2$ and $\boldsymbol{j} = \widehat{\psi}_0^*\nabla_{\boldsymbol{k}}\widehat{\psi}_0 - \widehat{\psi}_0\nabla_{\boldsymbol{k}}\widehat{\psi}_0^*$. If ψ_0 is real, then $\boldsymbol{j} = \boldsymbol{0}$ and the expression above reduces to $\ell^2(t) = \alpha t^2 + \ell^2(0)$.

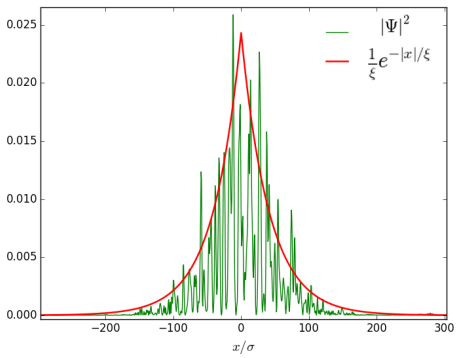

(a) Zoomed $|\psi|^2$ profile at t $\sim t_{max}$=400 in 1D.(M=4096, Δt=0.08, σ_g=61, V_0=0.8).

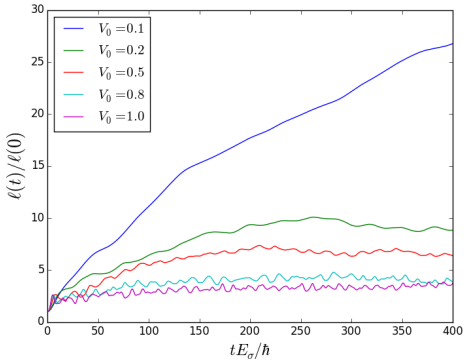

(b) Plot of $\ell(t)$ for different disorder strengths in 1D-system.(M=2048, Δt=0.02, σ_g=3)

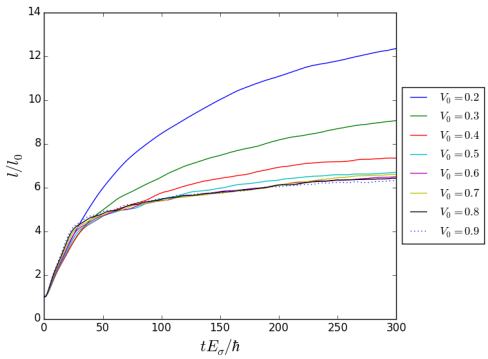

(c) Plot of $\ell(t)$ for different disorder strengths in 2D-system. (M=256, Δt=0.08, σ_g=3)

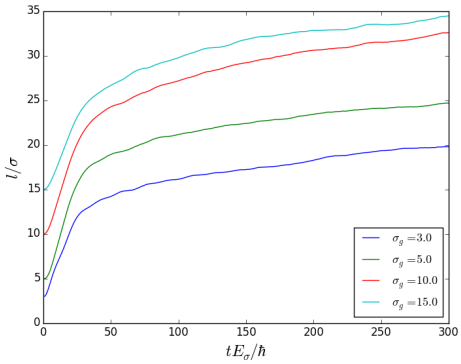

(d) Plot of $\ell(t)$ for different widths of the initial 2D-Gaussian wave packet. (M=256, Δt=0.08, V_0=0.7)

Fig. 4: Time evolution of the root-mean-square deviation, $\ell(t)$, for a given realization of disorder in one and two dimensions.

– is the signature of the phase changes induced in the wavefunction by the potential. They attenuate after statistical averaging over the disorder and are much less obvious in 2D systems, for which $\ell(t)$ is rather smooth (Fig. 4(c) and 4(d)).

By increasing the width of the initial Gaussian wave packet (Fig.4(d)), we increase the energy of the system and thus raise the upper-limit of $\ell(t)$-function (and consequently ξ).

The numerical tests have shown the conservation in time of the norm of ψ ($\langle\psi|\psi\rangle = \int \mathrm{d}^d\boldsymbol{r}|\psi(\boldsymbol{r},t)|^2$=1). The total energy $E(t) = {}_t\langle\psi|H|\psi\rangle_t = \int \mathrm{d}^d\boldsymbol{r}\left(|\nabla\psi(\boldsymbol{r},t)|^2 + V(\boldsymbol{r})|\psi(\boldsymbol{r},t)|^2\right)$ is also preserved (with negligible fluctuations). Studies on the influence of Δt step size on $\ell(t)$-function in 1D problem have shown that there is no perceptible difference between numerical solutions obtained for different $\Delta t \leqslant 0.1$. A strong divergence appears for $\Delta t > 0.5$. The value $\Delta t = 0.08$ or 0.1 is the most reasonable to solve the problem in $2D$.

5.3 Effects of Rashba spin-orbit interaction

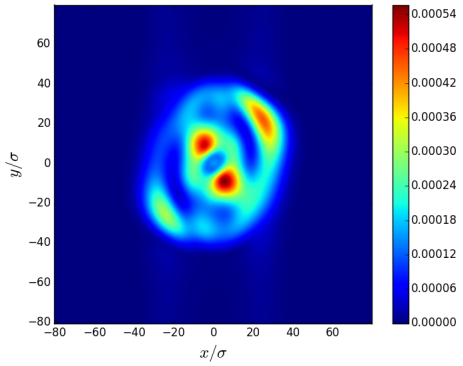

Fig. 5: $|\psi|^2$ distribution captured at time $t = 200\Delta t$ for a system which dynamics is governed by Rashba spin-orbit Hamiltonian H_{RSO}, without disorder. The result was obtained with M=256, Δt=0.1, σ_g=5 and λ=1.2.

Let $\psi_0 = \frac{1}{\sqrt{2}} \begin{pmatrix} \psi_{0_+} \\ \psi_{0_-} \end{pmatrix}$ be the initial state of the system. For the simplicity, we assume that $\psi_{0_+} = \psi_{0_-} = \phi_0$ where ϕ_0 is the Gaussian wave packet given by (8).

In the presence of solely Rashba-type spin-orbit coupling, the initial spinor ψ_0 extends in a way specific to the Hamiltonian $H_{RSO} = -\nabla^2 + \lambda\left(k_y\sigma_x - k_x\sigma_y\right)$. The corresponding probability density function $|\psi|^2 = |\psi_+|^2 + |\psi_-|^2$, plotted in Fig.5 at fixed time t, seems to admit a symmetric structure (that steel needs to be characterized). The corresponding root-mean-square displacement $\ell(t)$ diverges more rapidly then in case of free ballistic expansion (Fig.7(b)).

As shown in figure 6(a), the introduction of disorder breaks the existing symmetry and may limit drastically the wavefunction spread. The root-mean-square $\ell(t)$ may be fitted, as expected, by a function proportional to $\sqrt{t}$ (see Fig. 6(b)), provided that the degree of randomness is sufficiently large ($V_0 \lesssim 1$). Otherwise, the spin-orbit coupling effect prevails and $\ell(t)$ diverges stronger than $\sqrt{t}$ (see Fig.7).

From this we conclude that Rashba spin-orbit coupling has an antilocalization effect on 2D system in the presence of disorder.

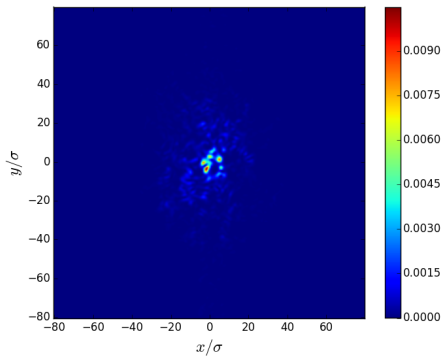

(a) $|\psi|^2$ profile captured at time $t = 200\Delta t$ for a system in the presence of spin-orbit coupling and the disorder ($H = H_{RSO} + V$)

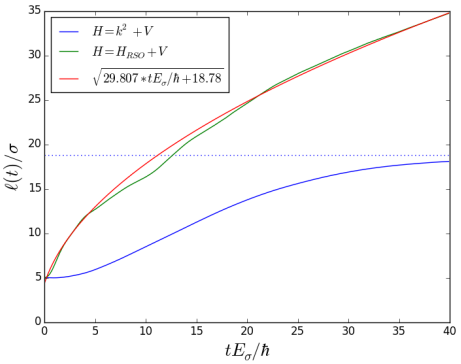

(b) Plot of $\ell(t)$ compared both to the function $f(t) = \sqrt{at + b}$ where $a = 29.807$ and $b = 18.780$ and to $\ell(t)$ obtained without spin-orbit coupling.

Fig. 6: Weak Anderson antilocalization induced by Rashba spin-orbit coupling in 2D disordered medium. Results obtained with M=256, Δt=0.1, V_0=0.7, σ_g=5 and λ=1.2.

The next step would be to find the set of parameters $\{V_0, \lambda\}$ in the neighbourhood of which emerges the transition between localized/anti-localized phase. The transition may probably be recognised by the strong divergence of the root-mean-square distance $\ell(t)$.

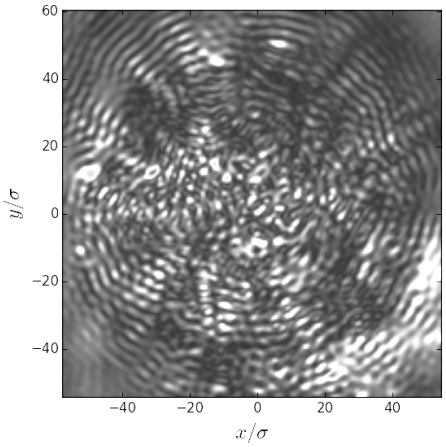

(a) Zoomed $|\psi|^2$ profile captured at $t = 150\Delta t$. $\lambda = 2,\ V_0 = 0.1$. The white regions correspond to the maximum of the intensity of $|\psi|^2$. (The condition $\psi \to 0$ as $|\boldsymbol{r}| \to \frac{L}{2}$ is well respected).

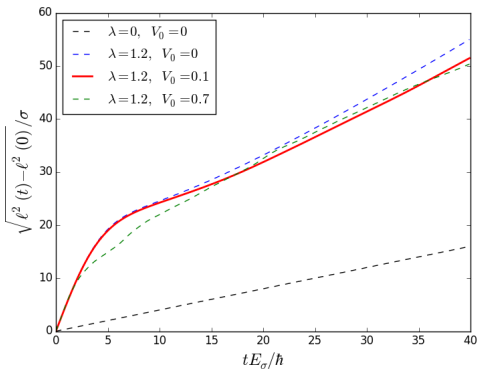

(b) Time evolution of $\sqrt{\ell^2(t) - \ell(0)}$ for $\lambda = 1.2$, $V_0 = 0.1$ (solid line) and its comparison to results obtained in ballistic, purely RSO-coupling and more or less diffusive regimes (dashed lines).

Fig. 7: Strong Anderson antilocalization induced by Rashba spin-orbit coupling in 2D disordered medium. Results obtained with M=512, Δt=0.1 and σ_g=5.

6 Conclusion

Guided by the experimental scenario, we have numerically built 1D and 2D optical blue-detuned speckle potential with realistic microscopic characteristics modelled by the correlation function $G_d(r)$. Using the split-step fft method, we have investigated the dynamics of a cloud of cold atoms exposed to the speckle field. In non interacting regime, one dimensional systems are exponentially localized. We have given an estimate for the localization length ξ in terms of an asymptotic value of the root-mean-square displacement $\ell(t)$. In two-dimensional systems, the convergence of $\ell(t)$ to a constant as $t \to +\infty$ is less rigorous: a long integration time and large system size are actually required to properly verify the existence of the localization, especially in the presence of weak disorder. The Rashba-type spin-orbit interaction has an antilocalization effect on the system. If it prevails over that of the disorder, the system is strongly antilocalized. Otherwise, the RSO-coupling leads to the existence of extended states, for which the root-mean-deviation is proportional to $\sqrt{t}$, as expected. Further numerical tests need to be performed to provide a set of parameters driving the Anderson transition.

References

[1] F. Evers and A. D. Mirlin, "Anderson transitions," *Reviews of Modern Physics*, vol. 80, pp. 1355–1417, Oct. 2008.

[2] H. D. Xie, *Anderson localization in disordered systems with competing channels*. Theses, Scuola Internazionale Superiore di Studi Avanzati, Oct. 2012.

[3] D. Delande, J. C. Garreau, L. Sanchez-Palencia, and B. V. Tiggelen, "La localisation forte d'Anderson," *Image de la physique*, pp. 70–74, 2009.

[4] D. S. Wiersma, P. Bartolini, A. Lagendijk, and R. Righini, "Localization of light in a disordered medium," *Nature*, vol. 390, pp. 671–673, Dec 1997.

[5] M. Störzer, P. Gross, C. M. Aegerter, and G. Maret, "Observation of the critical regime near anderson localization of light," *Phys. Rev. Lett.*, vol. 96, p. 063904, Feb 2006.

[6] T. Schwartz, G. Bartal, S. Fishman, and M. Segev, "Transport and anderson localization in disordered two-dimensional photonic lattices," *Nature*, vol. 446, pp. 52–55, Mar 2007.

[7] Y. Lahini, A. Avidan, F. Pozzi, M. Sorel, R. Morandotti, D. N. Christodoulides, and Y. Silberberg, "Anderson localization and nonlinearity in one-dimensional disordered photonic lattices," *Phys. Rev. Lett.*, vol. 100, p. 013906, Jan 2008.

[8] H. Hu, A. Strybulevych, J. H. Page, S. E. Skipetrov, and B. A. van Tiggelen, "Localization of ultrasound in a three-dimensional elastic network," *Nat Phys*, vol. 4, pp. 945–948, Dec 2008.

[9] A. A. Chabanov, M. Stoytchev, and A. Z. Genack, "Statistical signatures of photon localization," *Nature*, vol. 404, pp. 850–853, Apr 2000.

[10] G. Roati, C. D'Errico, L. Fallani, M. Fattori, C. Fort, M. Zaccanti, G. Modugno, M. Modugno, and M. Inguscio, "Anderson localization of a non-interacting bose-einstein condensate," *Nature*, vol. 453, pp. 895–898, Jun 2008.

[11] D. Delande and G. Orso, "Mobility Edge for Cold Atoms in Laser Speckle Potentials," *Physical Review Letters*, vol. 113, p. 060601, Aug. 2014.

[12] R. C. Kuhn, C. Miniatura, D. Delande, O. Sigwarth, and C. A. Müller, "Localization of matter waves in two-dimensional disordered optical potentials," *Phys. Rev. Lett.*, vol. 95, p. 250403, Dec 2005.

[13] P. Lugan, A. Aspect, L. Sanchez-Palencia, D. Delande, B. Grémaud, C. A. Müller, and C. Miniatura, "One-dimensional Anderson localization in certain correlated random potentials," *Physical Review A*, vol. 80, p. 023605, 2009.

[14] T. Prat, N. Cherroret, and D. Delande, "Semiclassical spectral function and density of states in speckle potentials," *ArXiv e-prints*, June 2016.

[15] M. Pasek, Z. Zhao, D. Delande, and G. Orso, "Phase diagram of the three-dimensional Anderson model for short-range speckle potentials," vol. 92, p. 053618, Nov. 2015.

[16] D. Bercioux and P. Lucignano, "Quantum transport in Rashba spin-orbit materials: a review," *Reports on Progress in Physics*, vol. 78, p. 106001, Oct. 2015.

[17] P. U. Suarez, "An introduction to the Split Step Fourier Method using MATLAB." January 18, 2013.

[18] T. Esslinger and F. Brennecke, "Exercises on BEC lecture - Problem Set 3." Spring term 2012, Swiss Federal Institute of Technology Zurich.

[19] P. W. Anderson, "Absence of diffusion in certain random lattices," *Phys. Rev.*, vol. 109, pp. 1492–1505, Mar 1958.

Appendices

A Code example for two dimensional system

```
# -*- coding: utf-8 -*-
import numpy as np
import matplotlib.pyplot as plt
from scipy.fftpack import fft2, ifft2, fftshift
from scipy.integrate import simps
import matplotlib.animation as animation

# Definition des fonctions

def TF2_transform(f, a):
    return (a**2)*fftshift(fft2(fftshift(f)))

def TF2_inverse(f, a):
    return (1./(a**2))*fftshift(ifft2(fftshift(f)))

def norm2(f):
    return np.real(f*np.conjugate(f))

def Heavside(X, Y, a):
    res0 = X**2 + Y**2
    n = np.size(X[0])
    res = np.zeros((n,n))
    for i in range(n):
        for j in range(n):
            if res0[i,j] <= a**2:
                res[i,j] = 1.
    return res

def Gauss2D(x1, x2, a):
    return np.exp(-(x1*x1 + x2*x2)/(2*a*a))/(2*np.pi*a*a)

# Mise en place d'une grille spatio-temporelle
# et d'une grille dans l'espace des {k}

M = 2**9           # nombre de points dans la grille
dx = 0.2*np.pi     # pas
dy = dx
L = M*dx           # longueur de l'intervalle selon x (= celui selon y)
n = np.arange(-M/2, M/2, 1)
x = dx*n
y = x
X,Y = np.meshgrid(x, y, indexing='ij')
xmax = x.max()
xmin = x.min()

dk = 2*np.pi/L   # pas dans l'espace de Fourier
kx = dk*n        # grille dans l'espace de Fourier
ky = kx
```

```
Kx, Ky = np.meshgrid(kx, ky, indexing='ij')
K2 = Kx*Kx + Ky*Ky
K4 = K2*K2

dt = 0.05          # pas temporel
tmax = 40.
t=np.arange(0., tmax, dt)
Q=np.size(t)

# Parametres :
numero_exp = 24      # (pour enregistement automatisee des donnes)
lambda_R = 1.        # constante de couplage spin-orbite
V0 = 0.2             # intensite du desordre
sigma_Gauss = 5.     # largeur du paquet d'onde initial

# Generation d'un potentiel desordonne (champ electrique A(x,y) ss dim)
A = np.random.normal(0,1., (M,M)) +1j*np.random.normal(0,1., (M,M))
k0 = 1.
sigma = 1./k0                # longueur de correlation
tfA = TF2_transform(A, dx) # transformee de Fourier de A
# redefinition de A avec correlation induite
A = TF2_inverse(tfA*Heavside(Kx, Ky, k0), dx)
V = norm2(A)                 # calcul de |A(x,y)|**2 pour tout x, y
meanV = np.mean(V)
V = (V/meanV - 1.)*V0

# Angle theta et phi
theta = np.zeros((M,M))
for j in range(M):
    for i in range(M/2):
        theta[i,j] = np.arctan(ky[j]/kx[i])
    theta[M/2,j] = np.pi*np.sign(ky[j])/2.
    for i in np.arange(M/2 + 1, M, 1):
        theta[i,j] = np.arctan(ky[j]/kx[i])

phi = theta - np.pi/2
# deux valeurs propres de T (en tout point (kx,ky))
lambda1 = K2 + lambda_R*np.sqrt(K2)
lambda2 = K2 - lambda_R*np.sqrt(K2)

# Definition de l'etat initial
psi0 = Gauss2D(X, Y, sigma_Gauss)
Iy0 = simps(psi0**2, x=x, axis = 0) # integration selon l'axe des x
I0 = simps(Iy0, x = y)              # integration selon l'axe des y
psi0 = psi0/np.sqrt(2*I0)           # renormalisation
PsiUp_0 = psi0
PsiDown_0 = psi0

# Calcul de Psi (par la methode split-step FFT symetrique
# procedure "V/2 - T - V/2", version non optimisee
PsiUp = np.zeros((Q, M, M), 'complex') # suite de Q matrices MxM
PsiDown = np.zeros((Q, M, M), 'complex')
# Initialisation
```

```
PsiUp[0, :, :] = PsiUp_0
PsiDown[0, :, :] = PsiDown_0

for q in range(Q-1):
    PsiUp_a = np.exp(-1j*V*dt/2.)*PsiUp[q,:,:]
    PsiDown_a = np.exp(-1j*V*dt/2.)*PsiDown[q,:,:]
    PsiUp_b_0 = TF2_transform(PsiUp_a, dx)
    PsiDown_b_0 = TF2_transform(PsiDown_a, dx)
    alpha_q = (PsiUp_b_0*np.exp(1j*phi) + PsiDown_b_0)/np.sqrt(2.)
    beta_q = (-PsiUp_b_0*np.exp(1j*phi) + PsiDown_b_0)/np.sqrt(2.)
    PsiUp_b = (alpha_q*np.exp(-1j*lambda1*dt)*np.exp(-1j*phi) - beta_q*np.exp(-1j*lambda2*dt)*np.exp(-1j*phi))/np.sqrt(2.)
    PsiDown_b = (alpha_q*np.exp(-1j*lambda1*dt) + beta_q*np.exp(-1j*lambda2*dt))/np.sqrt(2.)
    PsiUp_c = TF2_inverse(PsiUp_b, dx)
    PsiDown_c = TF2_inverse(PsiDown_b, dx)
    PsiUp[q+1,:,:] = np.exp(-1j*V*dt/2.)*PsiUp_c
    PsiDown[q+1,:,:] = np.exp(-1j*V*dt/2.)*PsiDown_c

Psi2 = norm2(PsiUp) + norm2(PsiDown)#suite de Q matrices MxM, |psi|^2(x,y, t_q)
NormePsi2x = simps(Psi2, x=y, axis=2)       # integration pour tout t selon y
NormePsi2 = simps(NormePsi2x, x=x, axis=1) # on obtient <Psi|Psi>(t)
Cmx = simps((X*X + Y*Y)*Psi2, x=y, axis=2)
Cm = simps(Cmx, x=x, axis=1)                # correspond a l^2(t)

# Animation 2D
fig = plt.figure(1)
ims = []
for q in np.linspace(0, Q-1, 400):
    im = plt.imshow(Psi2[int(q), :,:], cmap=plt.get_cmap('jet'), animated=True, aspect='equal', origin='lower',extent=(xmin,xmax,xmin,xmax))
    ims.append([im])

ani = animation.ArtistAnimation(fig, ims, interval=50, blit=True, repeat_delay=1000)
Writer = animation.writers['ffmpeg']
writer = Writer(fps=15, metadata=dict(artist='Me'), bitrate=1800)
ani.save('exp_%s_sigma_%s_V0_%s_tmax_%s_dt_%s_lambda_R_%s' %(numero_exp, sigma_Gauss, V0, tmax, dt, lambda_R), writer=writer)
plt.show()

plt.figure(2)
plt.imshow(Psi2[Q/2,:,:], cmap=plt.get_cmap('jet'), animated=True, aspect='equal', origin='lower',extent=(xmin,xmax,xmin,xmax))
plt.colorbar()
plt.xlabel(r'$x/\sigma$', size=18)
plt.ylabel(r'$y/\sigma$', size=18)

plt.figure(3) # plot de l(t)
plt.plot(t, np.sqrt(Cm), 'b')
plt.xlabel(r'$t E_{\sigma}/\hbar$', size=18)
```

```
147 plt.ylabel(r'$\ell$', size=18)

149 plt.figure(4) # verification de la conservation de la norme <psi|psi>(t)
    pour tout t
    plt.plot(t, NormePsi2)
151 plt.xlabel(r'$t E_{\sigma}/\hbar$', size=18)
    plt.ylabel(r'$<\Psi | \Psi>$', size = 18)
153 plt.ylim(0,1.5)
    plt.show()
```